

PAPER • OPEN ACCESS

Lateral Mn_5Ge_3 spin-valve in contact with a high-mobility Ge two-dimensional hole gas

To cite this article: David Weißhaupt *et al* 2024 *Semicond. Sci. Technol.* **39** 125004

View the [article online](#) for updates and enhancements.

You may also like

- [Novel GaN-based double-channel p-heterostructure field-effect transistors with a p-GaN insertion layer](#)
Xuerui Niu, , Bin Hou *et al.*
- [Analysis of back-gate effect on threshold voltage of p-channel GaN MOSFETs on polarization-junction substrates](#)
Takuya Hoshii, Akira Nakajima, Shin-ichi Nishizawa *et al.*
- [MOVPE-grown GaN/AlGaIn heterostructures on sapphire with polarization-induced two-dimensional hole gases](#)
Carsten Beckmann, Jens Wieben, Thorsten Zweipfennig *et al.*



ECS The Electrochemical Society
Advancing solid state & electrochemical science & technology






ECS UNITED

247th ECS Meeting
Montréal, Canada
May 18-22, 2025
Palais des Congrès de Montréal

Showcase your science!

Abstracts due December 6th

Lateral Mn_5Ge_3 spin-valve in contact with a high-mobility Ge two-dimensional hole gas

David Weißhaupt¹ , Christoph Sürgers^{2,*} , Dominik Bloos³, Hannes Simon Funk¹ , Michael Oehme¹, Gerda Fischer² , Markus Andreas Schubert⁵, Christian Wenger⁵, Joris van Slageren³ , Inga Anita Fischer⁴ and Jörg Schulze¹

¹ Institute of Semiconductor Engineering, University of Stuttgart, 70569 Stuttgart, Germany

² Physikalisches Institut, Karlsruhe Institute of Technology, 76131 Karlsruhe, Germany

³ Institute of Physical Chemistry, Pfaffenwaldring 55, 70569 Stuttgart, Germany

⁴ Experimental Physics and Functional Materials, Brandenburg University of Technology, 03046 Cottbus, Germany

⁵ Materials Research, IHP—Leibniz Institut für innovative Mikroelektronik, 15236 Frankfurt (Oder), Germany

E-mail: christoph.suergers@kit.edu

Received 12 March 2024, revised 23 September 2024

Accepted for publication 30 October 2024

Published 8 November 2024



Abstract

Ge two-dimensional hole gases (2DHG) in strained modulation-doped quantum-wells represent a promising material platform for future spintronic applications due to their excellent spin transport properties and the theoretical possibility of efficient spin manipulation. Due to the continuous development of epitaxial growth recipes extreme high hole mobilities and low effective masses can be achieved, promising an efficient spin transport. Furthermore, the Ge 2DHG can be integrated in the well-established industrial complementary metal-oxide-semiconductor (CMOS) devices technology. However, efficient electrical spin injection into a Ge 2DHG—an essential prerequisite for the realization of spintronic devices—has not yet been demonstrated. In this work, we report the fabrication and low-temperature magnetoresistance (MR) measurements of a laterally structured $\text{Mn}_5\text{Ge}_3/\text{Ge}$ 2DHG/ Mn_5Ge_3 device. The ferromagnetic Mn_5Ge_3 contacts are grown directly into the Ge quantum well by means of an interdiffusion process with a spacing of approximately 130 nm, forming a direct electrical contact between the ferromagnetic metal and the Ge 2DHG. Here, we report for the first time a clear MR signal for temperatures below 13 K possibly arising from successful spin injection into the high mobility Ge 2DHG. The results represent a step forward toward the realization of CMOS compatible spintronic devices based on a 2DHG.

Supplementary material for this article is available [online](#)

Keywords: magnetoelectronics, electrical spin injection, Ge 2DHG, Mn_5Ge_3 contacts, SiGe/Ge heterostructures

* Author to whom any correspondence should be addressed.



1. Introduction

New concepts summarized under the term ‘Beyond complementary metal-oxide-semiconductor (CMOS)’ are required in order to further increase the performance of semiconductor integrated circuits [1, 2]. One prominent example is the field of semiconductor spintronics where the electron spin is used in devices in addition to its charge [3–5]. For a viable spintronic device several requirements must be fulfilled. First, spins must be successfully injected into a high-conductivity channel. Second, the spin orientation must be maintained over a long distance, requiring in turn high charge carrier mobilities and long spin relaxation times. Third, there must be a means to efficiently manipulate the spin orientation. The spin-field-effect transistor (spin FET) proposed in 1990 by Datta and Das, is a prototypical semiconductor spintronics device [6] in which spin polarized charge carriers are injected from ferromagnetic source electrodes into a semiconductor channel. Depending on the relative orientation of the spin of the charge carriers and the magnetization of the drain electrode, the transistor is in its on- or off-state. The spin of the charge carrier is switched between the parallel and anti-parallel configuration relative to the magnetization of the ferromagnetic drain contact through the gate-controlled Rashba spin-orbit interaction resulting in an oscillating output characteristic that is unique for the spin FET and is largely determined by the giant magnetoresistance (GMR) effect [7, 8]. Thus, the Rashba effect enables spin-manipulation with the aid of an electrical field, which is an necessary requisite for the scalability and thus the integration of future spin-based devices into existing CMOS technology [9].

For efficient spin manipulation, materials lacking inversion symmetry and strong spin-orbit interaction generating a sizeable Rashba effect are required [10–13]. For potential industrial applications, the spin FET is discussed as a low-power transistor, since the energy for switching the spin orientation is orders of magnitude smaller than that of the Coulomb charging energy in a classic metal-oxide-semiconductor FET, thereby strongly reducing the heat dissipation in conventional semiconductor devices [14–16]. From a research point of view, the spin FET is of great interest because it does not only require electrical spin injection and spin detection as well as spin transport, but also spin manipulation by means of an electrical field. The unification of all components within one device makes it an ideal demonstrator and thus at the same time the foundation for future spintronic devices. However, the implementation of this device concept has proven to be extremely difficult. In their seminal paper, Datta and Das proposed that spin transport takes place in a buried high-mobility two-dimensional electron gas (2DEG) [6]. Even though Lee *et al* were able to demonstrate a working Si-based spin FET [17], there is only one example [18] where a non-local Rashba oscillation within an InAs 2DEG with ferromagnetic $\text{Ni}_{81}\text{Fe}_{19}$ contacts has been demonstrated. The main challenge is the fabrication of ferromagnetic contacts to

the buried channel without depleting the 2DEG. While various groups have reported successful electrical spin injection into buried 2DEGs in group III–V compound semiconductors [19–24], spin injection into a Si 2DEG was successfully demonstrated in only one study [25]. Unfortunately, the spin-orbit interaction in Si is comparably weak and materials with larger spin-orbit interactions are highly desired [26–28].

A promising and CMOS compatible material to meet all the requirements are Ge-based heterostructures forming a two-dimensional hole gas (2DHG) [29, 30]. In contrast to the 2DEG, the 2DHG provides an increased Rashba energy due to the larger spin-orbit interaction of holes compared to that of electrons giving rise to a more efficient spin manipulation [31]. On the one hand, large Rashba energies comparable to the group III–V compound semiconductors have been obtained by various methods such as weak anti-localization, magnetoresistance (MR), and cyclotron resonance measurements [32–38]. On the other hand, electronic transport is degraded by the fundamentally shorter spin relaxation time of holes compared to electrons. However, even if the exact relationship of spin-flip length on the momentum scattering is unclear, it is reasonable to assume that the spin orientation of holes is strongly linked to their momentum, so that the spin information is typically randomized with each scattering event. Consequently, the spin relaxation time of holes is of the same time scale as the transport scattering time [39, 40]. While the latter is commonly affected by large-angle scattering, the quantum scattering time considers each scattering event regardless of the scattering angle and can be used as a worst-case estimate for the spin relaxation time. Due to the ongoing development of growth recipes for the Ge 2DHGs, extremely high hole-mobilities and low effective masses have already been achieved resulting in enhanced transport and quantum scattering times for holes [41–44]. Therefore, the Ge 2DHG promises a high spin relaxation time and thus very good spin transport properties. In this respect it is remarkable that despite the good suitability of the Ge 2DHG for CMOS-compatible spintronic applications, electric spin injection into a Ge 2DHG has not been yet reported. So far, all spin injection experiments based on p-type material have been carried out on doped Ge bulk samples with three-terminal or four-terminal (4T) structures [45–52], which fundamentally differ in transport mechanism compared to a buried Ge 2DHG channel. Hence, exploring the spin manipulation and transport in a 2DHG, with a higher Rashba energy compared to a 2DEG, bears promising potential for spintronic applications.

Here, we report for the first time MR measurements performed on a lateral spin-valve device with a high-mobility Ge 2DHG as spin transport channel. The advantage of using Mn_5Ge_3 as a ferromagnetic material for potential spin injection is the low conductivity mismatch between the ‘bad metal’ Mn_5Ge_3 and the Ge 2DHG. The $\text{Ge}/\text{Si}_{1-x}\text{Ge}_x$ heterostructure was epitaxially grown on a (111) oriented Si substrate by molecular beam epitaxy. We used thin Mn_5Ge_3 layers as

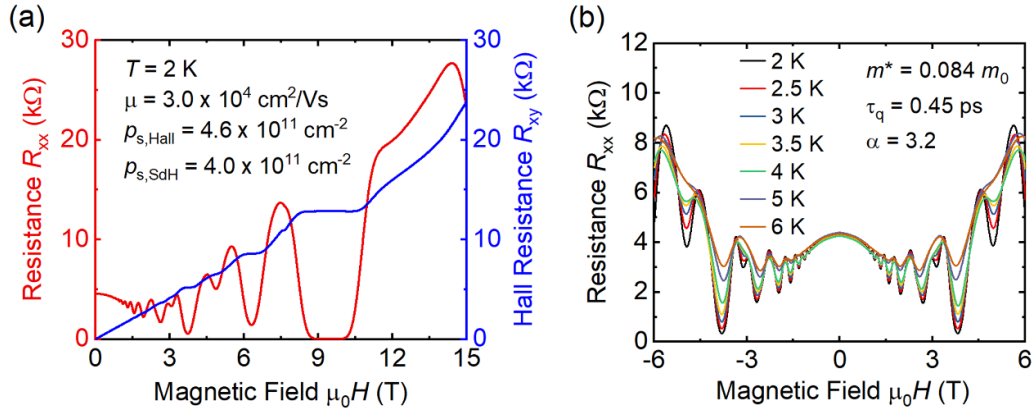


Figure 1. Transport properties of the Ge 2DHG: (a) longitudinal resistance R_{xx} and transverse Hall resistance R_{xy} vs. magnetic field μ_0H at $T = 2$ K. (b) Temperature dependence of R_{xx} .

ferromagnetic contacts, which were grown directly into the buried Ge quantum-well (QW) by means of interdiffusion. To this end, the entire $\text{Si}_{1-x}\text{Ge}_x$ capping layer above the Ge QW was removed prior to contact formation [53]. Temperature dependent MR measurements were first carried out on Hall bar structures to extract the quantum scattering time and effective mass as characteristic parameters for the spin transport properties. The magnetic properties were then analyzed using a superconducting quantum interference device (SQUID) magnetometer. Finally, the MR measurements on the structured devices exhibit signals hinting at spin injection into the Ge 2DHG. The GMR signal depends on the selected operating-point and could be observed up to a temperature of $T = 13$ K. The results reported in this work are important for the realization of CMOS compatible spintronic devices.

2. Device fabrication and characterization

2.1. Electronic transport properties of the Ge 2DHG

The Ge 2DHG was epitaxially grown on a Si (111) substrate following a standard growth protocol for the (100) substrate orientation reported earlier [54, 55]. The comprehensive crystal analysis by high resolution x-ray diffraction, transmission electron microscopy (TEM), atomic force microscopy of the grown Ge 2DHG sample, as well as the fabrication of the Hall bar and GMR device are provided in the supplemental material.

Figure 1(a) shows the longitudinal MR R_{xx} and the transverse Hall resistance R_{xy} in an applied magnetic field of up to $\mu_0H = 15$ T at a temperature of $T = 2$ K, from which a Hall mobility and Hall sheet carrier density of the Ge 2DHG of $\mu = (3.02 \pm 0.01) \times 10^4 \text{ cm}^2 \text{ V}^{-1} \text{ s}^{-1}$ and $p_{s,\text{Hall}} = (4.62 \pm 0.16) \times 10^{11} \text{ cm}^{-2}$, respectively, were obtained. There are indications for the presence of a fractional quantum Hall effect at high fields [56]. The corresponding temperature dependent Hall measurement is shown in the Supplemental Material. Figure 1(b) depicts the temperature dependence of the MR for a magnetic field range from $\mu_0H = -6$ T to $\mu_0H = 6$ T. Clear Shubnikov-de Haas (SdH)

oscillations and integer quantum Hall plateaus were observed, highlighting the quality of the epitaxially grown layers and therefore the good transport properties of the Ge 2DHG. The SdH oscillations start at approximately $\mu_0H = 0.65$ T, with spin splitting occurring at $\mu_0H = 3.13$ T. This is an indication for strong spin-orbit interaction and thus the possibility for efficient spin manipulation. Furthermore, the clear separation of the Landau levels for high magnetic fields gives further proof of the excellent transport properties of our samples. The symmetry of the MR curve excludes the presence of any inhomogeneities caused by, e.g. fluctuations in modulation doping [57].

A sheet carrier density $p_{s,\text{SdH}} = (4.00 \pm 0.30) \times 10^{11} \text{ cm}^{-2}$ was obtained from the period of the SdH oscillation and thus slightly deviates from the Hall measurement results. This difference indicates the presence of parasitic channels, which could either originate from the modulation-doped layer or from the Si substrate, which is relatively highly doped. However, since the relative amount of charge carriers outside the Ge 2DHG is quite small, the following GMR measurements are not affected. Furthermore, we observe a negative parabolic course of the longitudinal MR R_{xx} for small fields, which categorically excludes any strong parallel conductivity within our sample [58]. In existing literature, an upwards trend of the MR with increasing magnetic field is attributed to a parallel conductance and thus a parasitic sheet carrier density [59, 60].

From the temperature dependent damping of the amplitude of the SdH oscillations an effective mass of $m^* = (0.084 \pm 0.001) \times m_0$ (m_0 : electron mass) and a quantum-scattering time of $\tau_q = (0.45 \pm 0.01) \text{ ps}$ was extracted. At this point, we can estimate the spin-flip length l_{sf} using our experimentally determined transport data. In a worst-case scenario, we assume that the spin-information in the Ge 2DHG is randomized within each scattering event, i.e. the expected spin relaxation time τ_{sf} corresponds to the quantum scattering time τ_q . For the associated lower limit of the spin-flip length we then get $l_{\text{sf}} = \sqrt{D\tau_q} \approx (133.84 \pm 0.01) \text{ nm}$, where $D = (395.2 \pm 4.7) \text{ cm}^2 \text{ s}^{-1}$ is the diffusion constant of the holes in the Ge 2DHG.

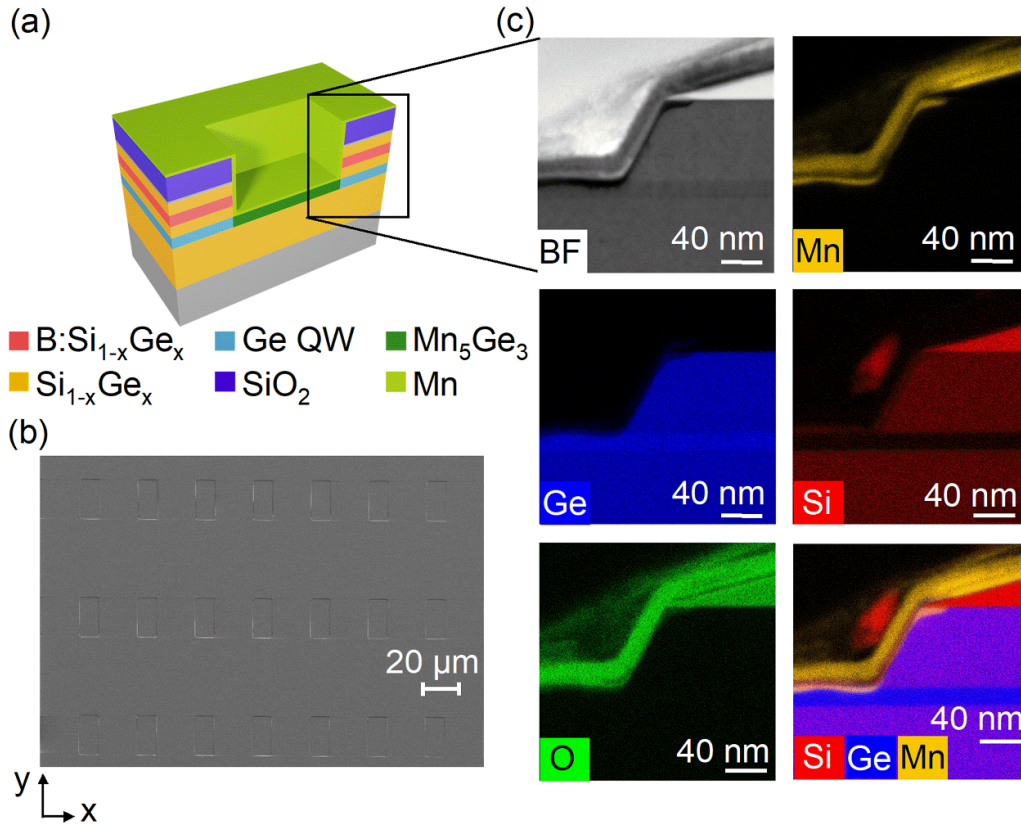


Figure 2. Structural properties of the Mn_5Ge_3 -contacts: (a) schematic cross-section of a single Mn_5Ge_3 contact. Further details are given in the supplemental material. (b) Top-view SEM-image section of the Mn_5Ge_3 contact array with a single Mn_5Ge_3 contact size of $A_1 = 10 \times 20 \mu\text{m}$. (c) Cross-sectional TEM and EDX images of a single Mn_5Ge_3 contact.

2.2. Ferromagnetic Mn_5Ge_3 contacts

The ferromagnetic Mn_5Ge_3 contacts were formed directly in the Ge QW using an interdiffusion process in order to establish a direct electrical contact between the ferromagnetic Mn_5Ge_3 and the Ge QW. Prior to the Mn_5Ge_3 contact formation, the entire $\text{Si}_{1-x}\text{Ge}_x$ capping layer on top of the Ge QW was removed using an Ar^+ ion milling process. The fabrication process and the magnetic properties of the ferromagnetic contacts have been already reported [53, 61, 62]. In particular, we have previously studied the formation of Mn_5Ge_3 by interdiffusion of evaporated Mn on Ge [61] and the contact formation from the Mn_5Ge_3 to the buried QW without formation of a tunneling barrier [53].

The ferromagnetic Mn_5Ge_3 contacts in this work were encapsulated with an additionally evaporated Mn protection layer. For the detection of electrical spin injection, we used two different lateral sizes of the Mn_5Ge_3 contact: $A = 5 \times 20 \mu\text{m}$ and $B = 10 \times 20 \mu\text{m}$. The Mn_5Ge_3 contacts were analysed by high-resolution TEM and energy-dispersive x-ray spectroscopy (EDX) using a Tecnai Osiris electron microscope from FEI operated at an acceleration voltage of 200 kV. EDX was performed in scanning mode using the software ‘Esprit’ from Bruker.

Figure 2(a) depicts the schematic cross-section of a single Mn_5Ge_3 contact and figure 2(c) the corresponding scanning TEM (STEM) and EDX images confirming that the Mn_5Ge_3

contact formed upon annealing is located directly within the Ge QW. The fabrication process leads to the formation of an additional $\text{Mn}_5(\text{Si}_{1-x}\text{Ge}_x)_3$ layer within the $\text{Si}_{1-x}\text{Ge}_x$ capping layer along the etched sidewall which creeps up to approximately $l = 20 \text{ nm}$ underneath the SiO_2 hard mask. However, these $\text{Mn}_5(\text{Si}_{1-x}\text{Ge}_x)_3$ layers do not create a short circuit below the SiO_2 layer between the center contacts and they also do not affect the contact separation distance since only the Ge 2DHG is conductive at low temperatures.

Figure 2(b) depicts the top-view scanning electron microscope (SEM) image of a Mn_5Ge_3 contact array with a single Mn_5Ge_3 contact size of $A_1 = 10 \times 20 \mu\text{m}$. For the magnetization measurements, the Mn_5Ge_3 contacts with the two different geometries ($A_1 = 10 \times 20 \mu\text{m}$, $A_2 = 5 \times 20 \mu\text{m}$.) were arranged as an array extended over an area of $3 \times 3 \text{ mm}$ and their data were compared with data obtained from an unstructured reference sample.

The magnetization measurements were performed with a SQUID magnetometer (MPMS, Quantum Design) with the y axis of the contacts, see figure 2(b) orientated along the in-plane external magnetic field. Figure 3(a) shows the temperature dependent in-plane magnetization for the different geometries in a magnetic field $\mu_0 H = 50 \text{ mT}$. For comparison, the magnetization curves are normalized with respect to their magnetic moment at a temperature of $T = 5 \text{ K}$. For all geometries, the temperature-dependent magnetization confirms the formation of ferromagnetic Mn_5Ge_3 layers.

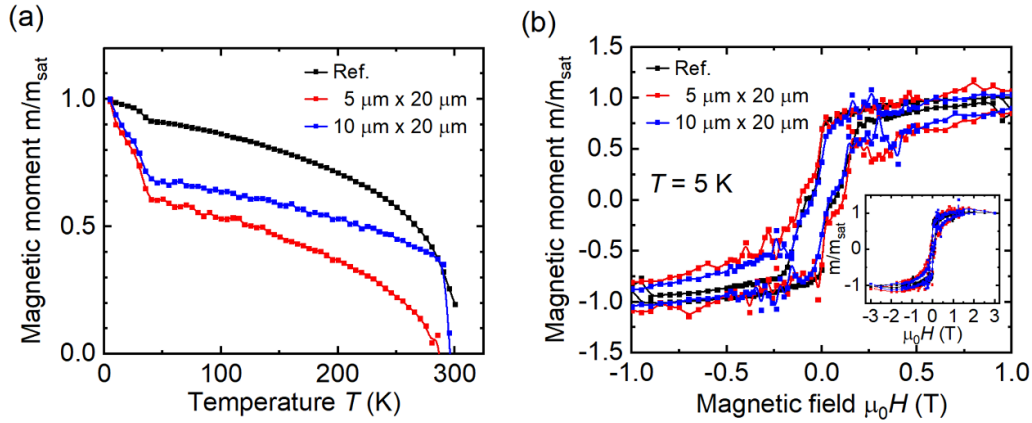


Figure 3. Magnetic properties of the Mn_5Ge_3 contacts with different geometries: (a) temperature dependent in-plane magnetization measured in an external magnetic field of $B = 50$ mT. (b) Corresponding in-plane magnetization curves at $T = 5$ K. For both measurements the external in-plane magnetic field was orientated along the y axis, see figure 3(b). Black curves represent data from the unstructured reference sample “Ref.”.

Independent of the geometry, we obtain a Curie temperature of about 300 K. Among the possible compounds of Mn and Ge that can form, only Mn_5Ge_3 is ferromagnetic with a Curie temperature around $T = 300$ K and exhibits no other magnetic phase transition [63, 64]. However, we observe a strong change of the slope of the magnetization at a temperature of about $T = 40$ K, which arises from the $\text{Mn}_5(\text{Si}_{1-x}\text{Ge}_x)_3$ layer that was additionally generated within the $\text{Si}_{1-x}\text{Ge}_x$ capping layer along the etched sidewall [62]. The respective magnetization curves measured at a temperature of $T = 5$ K are shown in figure 3(b). The inset depicts the same data up to maximum external field to $\mu_0H = 3$ T. The curves were corrected for a diamagnetic background signal arising from the semiconductor substrate and the sample holder. Again, for comparison all magnetization curves are normalized with respect to their saturation magnetic moments. We observe a double hysteresis at $T = 5$ K, which again can be explained by the overlay of the Mn_5Ge_3 layer with the $\text{Mn}_5(\text{Si}_{1-x}\text{Ge}_x)_3$ layer. The obtained coercive fields are $\mu_0H_C = (116 \pm 10)$ mT, $\mu_0H_C = (46 \pm 10)$ mT, and $\mu_0H_C = (73 \pm 10)$ mT for the geometries of $A_2 = 5 \times 20 \mu\text{m}$, $A_1 = 10 \times 20 \mu\text{m}$, and the unstructured reference sample, respectively. The direct comparison of the two geometries A_1 and A_2 indicates magnetic hardening, i.e. an increase in coercivity for the A_2 sample which is in line with the general increase of the intrinsic coercivity with decreasing particle size for multidomain particles. From a magnetic point of view, the ferromagnetic Mn_5Ge_3 contacts meet the magnetic requirements for the detection of electrical spin injection and thus can be used for further experiments.

2.3. Measurements on the GMR device

Figure 4 gives a schematic overview of the GMR device with spin transport in the Ge 2DHG taking place between two ferromagnetic Mn_5Ge_3 contacts.

The MR measurements on the GMR device were performed in a physical property measurement system (Quantum Design) for various temperatures and magnetic fields oriented in the plane of the sample and parallel to the long side of the Mn_5Ge_3

electrodes, i.e. along the y axis (figure 4). A DC voltage V_{DC} was modulated by an alternating currents (AC) voltage V_{AC} of frequency $f_{\text{ref}} = 321.7$ Hz and amplitude of a few percent of V_{DC} applied to the device under test, generating currents I_{DC} and I_{AC} , in series with a resistor $R_{\text{ref}} = 1$ k Ω and an I - V converter (FEMTO DLCPA200) with a gain of 10^3 . The current I_{DC} through the device was determined from the voltage drop V_{ref} across R_{ref} measured with a Keithley 2182 voltmeter. The differential resistance $dR = dV/dI$ was determined by two lock-in amplifiers (Stanford Research Systems SRS 830) synchronously coupled to f_{ref} and measuring the voltage dV across the device and a signal proportional to dI at the output of the I - V converter. In addition, the DC resistance was determined by the voltage drop across the device measured with a Keithley 2182 voltmeter divided by I_{DC} .

3. Results and discussion

The device comprises four ferromagnetic Mn_5Ge_3 electrodes in contact with the semiconducting Ge 2DHG transport channel, with spin transport taking place between the two center contacts separated by a distance lower than the spin-diffusion-length. A detailed description of the fabrication process of the device is available in the supplemental material. Figure 4 shows the schematic cross section of the final device together with top-view SEM images of the inner contacts (contacts 2, 3, and 4) with different magnification. The Mn_5Ge_3 contacts formed by the interdiffusion process act as barriers in the Ge channel for the 2DHG. Therefore, the standard non-local measurement approach where the current is applied between contacts 2 and 3 and the voltage is measured between contacts 4 and 5 (see figure 4) to verify spin injection, cannot be performed with the present device. Hence, we follow the same approach as adopted in [25, 63], where superimposed DC and AC are applied between the outer contacts (contact 2 and 5) and the AC voltage between the inner contacts (contact 3 and 4) is measured. The DC current serves to bring the

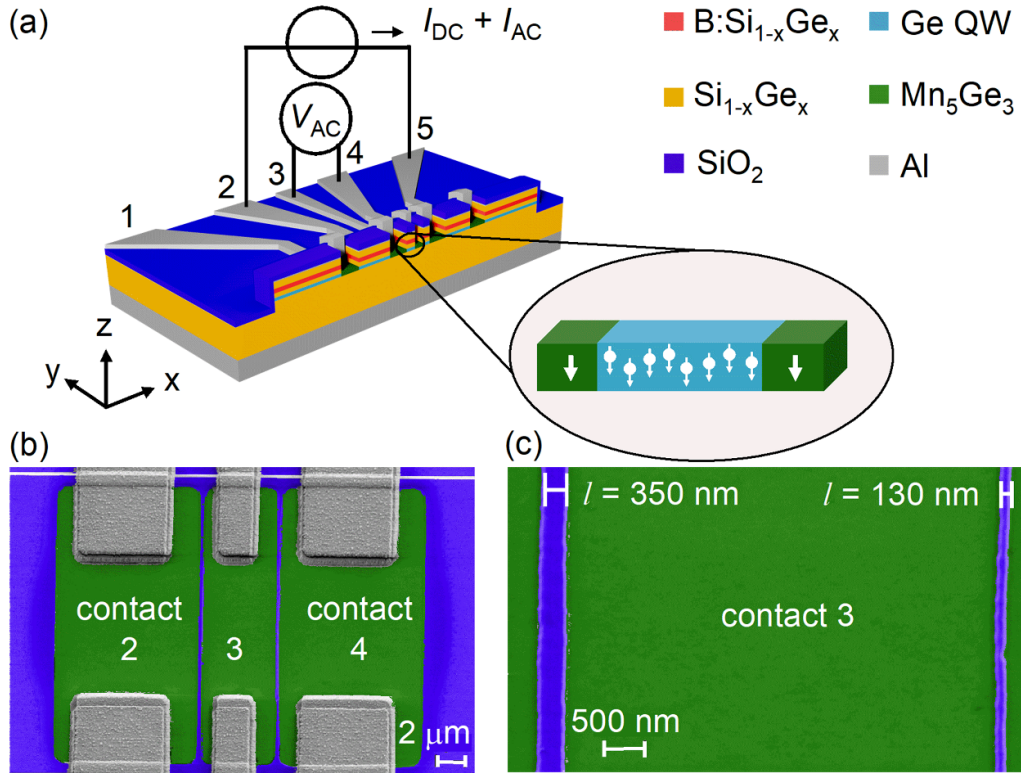


Figure 4. (a) Schematic illustration of the device structure used for the GMR measurements in this study. The spins are electrically injected and detected using ferromagnetic Mn_5Ge_3 contacts. The spin transport takes place in the Ge QW which accommodates a high mobility 2DHG. (b) and (c) show the top-view SEM images of the surface with different magnifications. In (c), the Mn_5Ge_3 contacts are well separated by distances of 350 nm and only 130 nm between contacts 2 and 3, and between contacts 3 and 4, respectively.

device to a suitable operation point (see below) and the AC current serves for the actual measurement.

Furthermore, the final design of the device differs from the well-established 4T-Hanle structure in that five contacts are used instead of four allowing spin-transport measurements over two different distances within one device. The two distances between the center electrode and the outer right or left electrode are approximately $l = 130$ nm and $l = 350$ nm, respectively, see figure 4. The size of the Mn_5Ge_3 center contact is $A_2 = 5 \mu\text{m} \times 20 \mu\text{m}$, all other contacts are twice as wide with a size of $A_1 = 10 \mu\text{m} \times 20 \mu\text{m}$.

Figure 5(a) shows MR curves $dR = dV/dI$ of the $\text{Mn}_5\text{Ge}_3/\text{Ge}$ 2DHG/ Mn_5Ge_3 device with a channel length of $l = 130$ nm at a temperature of $T = 2$ K for different DC currents I_{DC} . While no signal was measured for small DC currents, a clear GMR signal develops as the DC current I_{DC} increases. For $I_{\text{DC}} = 24 \mu\text{A}$ and $V_{\text{DC}} = 6$ V, corresponding to a resistance $R = 250$ k Ω , a $dR = 8.9$ k Ω and a MR of $dR/R = 3.6\%$ were obtained. A dependence of the electric spin injection on the applied DC current has already been reported for configurations involving $\text{Mn}_5\text{Ge}_3/\text{Ge}$ [65] and $\text{Mn}_5(\text{Si}_{1-x}\text{Ge}_x)_3/\text{Si}$ [25] contacts and has been attributed to the fact that the Mn_5Ge_3 contact on the Ge surface forms a Schottky barrier with a barrier height of $\phi_B = 0.25$ eV [66] which blocks electric spin injection. When a sufficiently high bias is applied to the Schottky contact, spin polarized holes can tunnel through the Schottky barrier, which becomes narrower

at higher bias. This leads to the formation of spin polarized currents in the Ge 2DHG. The spin polarized electrons then migrate in the Ge 2DHG to the second ferromagnetic contact. During this process the spin polarization decays exponentially due to scattering. The relative orientation between the spins in the Ge 2DHG and the magnetization of the second Mn_5Ge_3 contact then defines the total resistance and thus the signal structure.

Sweeping the external magnetic field leads to switching of the magnetization between the parallel and anti-parallel configurations of the two ferromagnetic Mn_5Ge_3 contacts. For large external magnetic fields, the magnetization of the two Mn_5Ge_3 contacts follows the direction of the external field, i.e. their mutual orientation is parallel. When the direction of the magnetic field changes in the reversed direction, the different coercive fields of the two electrodes cause the magnetization in the contacts to switch at different absolute field strengths. In our sample, the low spatial separation between the middle ferromagnetic contacts can be expected to result in a sizeable antiferromagnetic coupling between neighbouring contacts due to dipole-dipole interactions. Our MR signal, therefore, shows a different dependence on the external magnetic field than for 4T-Hanle structures with larger contact spacing, which usually exhibits GMR behaviour with separated MR hysteresis. When sweeping the amplitude of the in-plane external magnetic field from large positive values to large negative values, we obtain a change in our MR signal already at

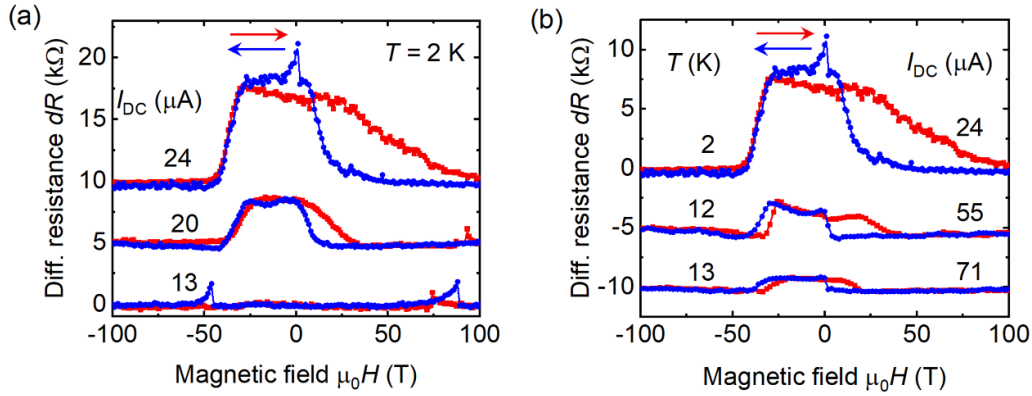


Figure 5. MR measurements of the $\text{Mn}_5\text{Ge}_3/\text{Ge}$ 2DHG/ Mn_5Ge_3 device with a channel length of $l = 130$ nm. (a) GMR signal for different DC currents I_{DC} at $T = 2$ K. (b) GMR signal at different temperatures with an adjusted operating point I_{DC} . For the sake of clarity, a constant MR has been removed from the raw data and the measurements are shifted with respect to each other.

small positive values of the external field instead of at small negative values, indicating anti-parallel orientation of the magnetization in the neighbouring contacts prior to the sign change of the magnetic field.

The GMR signal is shifted towards negative external fields by about $\Delta\mu_0H = (-20 \pm 10)$ mT. Such shifting is typically caused by a coupling of the ferromagnet with an anti-ferromagnetic thin film, known as the exchange-bias effect [67]. In our samples, the generation of local changes in alloy composition during the annealing step for the formation of the Mn-based ferromagnetic contacts could lead to this effect [62]. Indeed, the magnetic hysteresis curves for the geometries of $A_2 = 5 \times 20 \mu\text{m}$, $A_1 = 10 \times 20 \mu\text{m}$, and the unstructured reference sample, presented in figure 3(b), indicate the presence of a small shift in magnetic field by approximately $\Delta\mu_0H = (-5 \pm 10)$ mT, $\Delta\mu_0H = (-13 \pm 10)$ mT, and $\Delta\mu_0H = (-19 \pm 10)$ mT, respectively. However, it is more likely that the strongly enhanced demagnetization fields in microstructured samples may also lead to an antiferromagnetic coupling and a strongly field-shifted GMR behaviour [66]. A similar behaviour has been observed for lateral 2-terminal structures on the $\text{Si}_{0.1}\text{Ge}_{0.9}$ platform when sweeping a minorloop [68]. Hence, independent of the origin of the shifted GMR characteristics the DC current dependent GMR signals provide strong evidence for successful spin injection, transport, and detection in the Ge 2DHG.

Figure 5(b) shows the GMR signal for different temperatures. For this purpose, the operating point I_{DC} was chosen so that the relative signal for the respective temperature is at its maximum. The signal is significantly attenuated with increasing temperature, which is in good agreement with the results of the magnetotransport measurements, i.e. the SdH oscillations are strongly damped in the range from $T = 2$ K to $T = 6$ K, indicating an increase in scattering with increasing temperature. Although the GMR signal is already strongly reduced at 13 K, the data obtained on a prototype system provide the first evidence for spin injection into a high-mobility 2DHG.

Overall, the GMR signal could only be observed for a short distance of $l = 130$ nm between the electrodes. The sample with a larger electrode distance of $l = 350$ nm

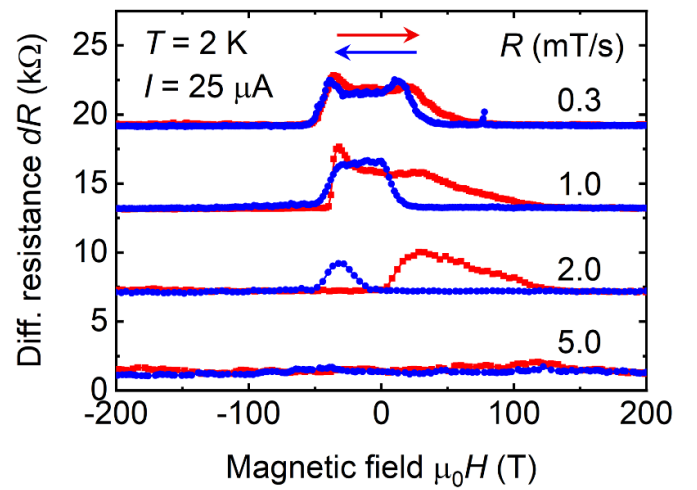


Figure 6. MR measurements for different sweep rates R of the external magnetic field at $T = 2$ K and for an applied DC current is $I_{\text{DC}} = 25 \mu\text{A}$. A constant MR has been removed from the raw data and the various measurements are shifted for clarity.

shows no evidence of spin injection (not shown), which means that the associated spin-flip length is expected to be somewhere between these two distances. Thus, the lower limit spin-flip length of about $l_{\text{sf}} = (133.84 \pm 0.01)$ nm calculated on the basis of the quantum-scattering time is in good agreement with the experimental results presented here.

The MR measurements presented in figure 5 were performed at a fixed sweep rate of the external magnetic field of $R = 0.2 \text{ mT s}^{-1}$. However, our experiments have shown that the sweep rate has a decisive influence on the signal structure. Figure 6 compares the MR-curves for different sweep rates of the external magnetic field. The measurements shown were carried out at a temperature $T = 2$ K with an applied DC current of $I_{\text{DC}} = 25 \mu\text{A}$. The GMR signal only appears for sweep rates below $R < 1.0 \text{ mT s}^{-1}$, whereas no signal structure can be observed for high sweep rates of $R = 5.0 \text{ mT s}^{-1}$. MR measurements with sweep rates in the range of $1.0 \text{ mT s}^{-1} \leq$

$R \leq 5.0 \text{ mT s}^{-1}$ show signal structures resembling spin-valve signals. This dependence on the sweep rate of the external magnetic field results from the switching dynamics behavior of the ferromagnetic Mn_5Ge_3 contacts. The alignment of the magnetization or the individual domains in the external magnetic field does not take place instantaneously, but is also retarded with a certain time constant. Sweep rates that are too fast lead to a modification of the GMR signal, since the individual domains cannot follow the rapidly changing external magnetic field. This influence of the magnetic field sweep rate on magnetic transitions has already been observed for synthetic ferrimagnets with large lateral size and could also explain our observation. Thus, modifying the sweep rate leads to change of the magnetization reversal process from domain wall propagation to nucleation, the latter dominating at a high sweeping rate [69]. The spin-valve-like signal for 2.0 mT s^{-1} therefore corresponds to a GMR signal which shifts on the magnetic field axis with decreasing sweep rate until both measurements match. For sweep rates higher than $R = 5.0 \text{ mT s}^{-1}$, there is no longer any defined magnetic switching behavior, which is why no change in resistance can be detected electrically.

4. Conclusion

Low-temperature MR measurements performed on a lateral ferromagnet/Ge 2DHG/ferromagnet device structure show a clear GMR signal for a contact distance of 130 nm between the electrodes. For this purpose, we use ferromagnetic Mn_5Ge_3 contacts directly grown as a thin film into the Ge QW to establish a good electrical contact between the Mn_5Ge_3 contact and the Ge 2DHG. Depending on the DC current I_{DC} , we observe GMR signals up to a temperature of $T = 13 \text{ K}$. The attenuation of the GMR signal with increasing temperature is in agreement with the quantum-mechanical transport properties of the Ge 2DHG. The results provide first evidence of electrical spin injection from a ferromagnet into a high-mobility Ge 2DHG. This is an important step toward the realization of future CMOS compatible spintronic devices, in particular for devices based on the spin FET proposed by Datta and Das. Future research is needed to improve the fabrication process and materials properties by reducing the lateral contact separation or increasing the spin flip length in order to observe this behavior at higher temperatures for potential applications.

Data availability statement

The data cannot be made publicly available upon publication because the cost of preparing, depositing and hosting the data would be prohibitive within the terms of this research project. The data that support the findings of this study are available upon reasonable request from the authors.

Acknowledgment

We acknowledge funding by the Deutsche Forschungsgemeinschaft (DFG) under Grants FI 1511/3-1 & SU 225/3-1 as well

by the Center for Integrated Quantum Science & Technology (IQST). D B and J V S thank the Ministry of Science, Research and Art Baden-Württemberg (MWK) as well as the University of Stuttgart for funding (Research Seed Capital).

ORCID iDs

David Weißhaupt  <https://orcid.org/0000-0001-5754-7793>
 Christoph Sürgers  <https://orcid.org/0000-0002-2132-9775>
 Hannes Simon Funk  <https://orcid.org/0000-0001-8485-2400>
 Gerda Fischer  <https://orcid.org/0000-0002-7545-1995>
 Joris van Slageren  <https://orcid.org/0000-0002-0855-8960>

References

- [1] Moore G E 2006 Cramming more components onto integrated circuits, Reprinted from Electronics, volume 38, number 8, April 19, 1965, pp.114 ff., *IEEE Solid-State Circuits Society Newsletter* **11** 33
- [2] Sugahara S and Nitta J 2010 Spin-transistor electronics: an overview and outlook *Proc. IEEE* **98** 2124
- [3] Wolf S A, Awschalom D D, Buhrman R A, Daughton J M, von Molnár S, Roukes M L, Chtchelkanova A Y and Treger D M 2001 Spintronics: a spin-based electronics vision for the future *Science* **294** 1488
- [4] Žutić I, Fabian J and Das Sarma S 2004 Spintronics: fundamentals and applications *Rev. Mod. Phys.* **76** 323
- [5] Jansen R 2012 Silicon spintronics *Nat. Mater.* **11** 400
- [6] Datta S and Das B 1990 Electronic analog of the electro-optic modulator *Appl. Phys. Lett.* **56** 665
- [7] Baibich M N, Broto J M, Fert A, Nguyen Van Dau F, Petroff F, Etienne P, Creuzet G, Friederich A and Chazelas J 1988 Giant magnetoresistance of (001)Fe/(001)Cr magnetic superlattices *Phys. Rev. Lett.* **61** 2472
- [8] Binasch G, Grünberg P, Saurenbach F and Zinn W 1989 Enhanced magnetoresistance in layered magnetic structures with antiferromagnetic interlayer exchange *Phys. Rev. B* **39** 4828
- [9] Bercieux D and Lucignano P 2015 Quantum transport in Rashba spin-orbit materials: a review *Rep. Prog. Phys.* **78** 106001
- [10] Bychkov Y A and Rashba E I 1984 Oscillatory effects and the magnetic susceptibility of carriers in inversion layers *J. Phys. C* **17** 6039
- [11] Lommer G, Malcher F and Rossler U 1988 Spin splitting in semiconductor heterostructures for B-0 *Phys. Rev. Lett.* **60** 728
- [12] Das B, Miller D C, Datta S, Reifenberger R, Hong W P, Bhattacharya P K, Singh J and Jaffe M 1989 Evidence for spin splitting in In_xGa *Phys. Rev. B* **39** 1411
- [13] Luo J, Munekata H, Fang F F and Stiles P J 1990 Effects of inversion asymmetry on electron energy band structures in GaSb/InAs/GaSb quantum wells *Phys. Rev. B* **41** 7685
- [14] Nikonov D E, Bourianoff G I and Gargini P A 2007 Power dissipation in spintronic devices out of thermodynamic equilibrium *J. Supercond. Novel Magn.* **19** 497
- [15] Awschalom D D and Flatté M E 2007 Challenges for semiconductor spintronics *Nat. Phys.* **3** 153
- [16] Hall K C and Flatté M E 2006 Performance of a spin-based insulated gate field effect transistor *Appl. Phys. Lett.* **88** 162503
- [17] Lee S, Koike H, Goto M, Miwa S, Suzuki Y, Yamashita N, Ohshima R, Shigematsu E, Ando Y and Shiraishi M 2021

- Synthetic Rashba spin-orbit system using a silicon metal-oxide semiconductor *Nat. Mater.* **20** 1228
- [18] Koo H C, Kwon J H, Eom J, Chang J, Han S H and Johnson M 2009 Control of spin precession in a spin-injected field effect transistor *Science* **325** 1515
- [19] Koo H C, Yi H, Ko JB, Chang J, Han SH, Jung D, Huh SG and Eom J 2007 Electrical spin injection and detection in an InAs quantum well *Appl. Phys. Lett.* **90** 22101
- [20] Oltscher M, Ciorga M, Utz M, Schuh D, Bougeard D and Weiss D 2014 Electrical spin injection into high mobility 2D systems *Phys. Rev. Lett.* **113** 236602
- [21] Chang J, Cheol Koo H, Eom J, Hee Han S and Johnson M 2011 Injection, detection and gate voltage control of spins in the spin field effect transistor *J. Appl. Phys.* **109** 102405
- [22] Koo H C, Kwon J H, Eom J, Chang J, Han S H and Johnson M 2011 Gate modulation of spin precession in a semiconductor channel *J. Phys. D: Appl. Phys.* **44** 64006
- [23] Ciorga M 2016 Electrical spin injection and detection in high mobility 2DEG systems *J. Phys.: Condens. Matter* **28** 453003
- [24] Zhang X et al 2021 Electrical spin injection into the 2D electron Gas in AlN/GaN heterostructures with ultrathin AlN tunnel barrier *Adv. Funct. Mater.* **31** 2009771
- [25] Chang LT et al 2016 Electrical detection of spin transport in Si two-dimensional electron gas systems *Nanotechnology* **27** 365701
- [26] Ganguly A, Kondou K, Sukegawa H, Mitani S, Kasai S, Niimi Y, Otani Y and Barman A 2014 Thickness dependence of spin torque ferromagnetic resonance in Co 75 Fe 25 /Pt bilayer films *Appl. Phys. Lett.* **104** 72405
- [27] Liu L, Moriyama T, Ralph D C and Buhrman R A 2011 Spin-torque ferromagnetic resonance induced by the spin Hall effect *Phys. Rev. Lett.* **106** 036601
- [28] Pai C F, Liu L, Li Y, Tseng H W, Ralph D C and Buhrman R A 2012 Spin transfer torque devices utilizing the giant spin Hall effect of tungsten *Appl. Phys. Lett.* **101** 122404
- [29] Morrison C and Myronov M 2016 Strained germanium for applications in spintronics *Phys. Status Solidi a* **213** 2809
- [30] Scappucci G, Kloeffel C, Zwanenburg F A, Loss D, Myronov M, Zhang J J, de Franceschi S, Katsaros G and Veldhorst M 2021 The germanium quantum information route *Nat. Rev. Mater.* **6** 926
- [31] Gvozdić D M, Ekenberg U and Thylén L 2006 Comparison of performance of n- and p-type spin transistors with conventional transistors *J. Supercond. Novel Magn.* **18** 349–56
- [32] Chou C T, Jacobson N T, Moussa J E, Baczewski A D, Chuang Y, Liu C Y, Li J Y and Lu T M 2018 Weak anti-localization of two-dimensional holes in germanium beyond the diffusive regime *Nanoscale* **10** 20559–64
- [33] Moriya R et al 2014 Cubic Rashba spin-orbit interaction of a two-dimensional hole gas in a strained-Ge/SiGe quantum well *Phys. Rev. Lett.* **113** 086601
- [34] Foronda J, Morrison C, Halpin J E, Rhead S D and Myronov M 2015 Weak antilocalization of high mobility holes in a strained germanium quantum well heterostructure *J. Phys.: Condens. Matter* **27** 22201
- [35] Morrison C, Wiśniewski P, Rhead S D, Foronda J, Leadley D R and Myronov M 2014 Observation of Rashba zero-field spin splitting in a strained germanium 2D hole gas *Appl. Phys. Lett.* **105** 182401
- [36] Morrison C, Foronda J, Wiśniewski P, Rhead S D, Leadley D R and Myronov M 2016 Evidence of strong spin-orbit interaction in strained epitaxial germanium *Thin Solid Films* **602** 84–89
- [37] Failla M, Myronov M, Morrison C, Leadley D R and Lloyd-Hughes J 2015 Narrow heavy-hole cyclotron resonances split by the cubic Rashba spin-orbit interaction in strained germanium quantum wells *Phys. Rev. B* **92** 045303
- [38] Failla M et al 2016 Terahertz quantum Hall effect for spin-split heavy-hole gases in strained Ge quantum wells *New J. Phys.* **18** 113036
- [39] Winkler R 2003 *Spin-orbit Coupling Effects in Two-dimensional Electron and Hole Systems* (Springer)
- [40] Dyakonov M I 2017 *Spin Physics in Semiconductors (Springer Series in Solid State Sciences)* (Springer)
- [41] Dobbie A, Myronov M, Morris R J H, Hassan A H A, Prest M J, Shah V A, Parker E H C, Whall T E and Leadley D R 2012 Ultra-high hole mobility exceeding one million in a strained germanium quantum well *Appl. Phys. Lett.* **101** 172108
- [42] Myronov M, Morrison C, Halpin J, Rhead S, Foronda J and Leadley D 2015 Revealing high room and low temperatures mobilities of 2D holes in a strained Ge quantum well heterostructures grown on a standard Si(0 0 1) substrate *Solid-State Electron.* **110** 35–9
- [43] Shi Q, Zudov M A, Morrison C and Myronov M 2015 Spinless composite fermions in an ultrahigh-quality strained Ge quantum well *Phys. Rev. B* **91** 241303(R)
- [44] Shi Q, Zudov M A, Morrison C and Myronov M 2015 Strong transport anisotropy in Ge/SiGe quantum wells in tilted magnetic fields *Phys. Rev. B* **91** 201301(R)
- [45] Jeon K R, Min B C, Jo Y H, Lee H S, Shin I J, Park C Y, Park S Y and Shin S C 2011 Electrical spin injection and accumulation in CoFe/MgO/Ge contacts at room temperature *Phys. Rev. B* **84** 165315
- [46] Hanbicki A T, Cheng S F, Goswami R, van't Erve O and Jonker B T 2012 Electrical injection and detection of spin accumulation in Ge at room temperature *Solid State Commun.* **152** 244
- [47] Fischer I A, Chang L T, Sürgers C, Rolseth E, Reiter S, Stefanov S, Chiussi S, Tang J, Wang K L and Schulze J 2014 Hanle-effect measurements of spin injection from Mn 5Ge3C0.8/Al2O3 -contacts into degenerately doped Ge channels on Si *Appl. Phys. Lett.* **105** 222408
- [48] Spiesser A, Saito H, Jansen R, Yuasa S and Ando K 2014 Large spin accumulation voltages in epitaxial Mn5Ge3 contacts on Ge without an oxide tunnel barrier *Phys. Rev. B* **90** 205213
- [49] Chang LT, Han W, Zhou Y, Tang J, Fischer I A, Oehme M, Schulze J, Kawakami R K and Wang K L 2013 Comparison of spin lifetimes in n -Ge characterized between three-terminal and four-terminal nonlocal hanle measurements *Semicond. Sci. Technol.* **28** 15018
- [50] Zhou Y, Han W, Chang L T, Xiu F, Wang M, Oehme M, Schulze J, Kawakami R K and Wang K L 2011 Electrical spin injection and transport in germanium *Phys. Rev. B* **84** 125323
- [51] Kasahara K, Fujita Y, Yamada S, Sawano K, Miyao M and Hamaya K 2014 Greatly enhanced generation efficiency of pure spin currents in Ge using heusler compound Co2 FeSi electrodes *Appl. Phys. Express* **7** 33002
- [52] Iba S, Saito H, Spiesser A, Watanabe S, Jansen R, Yuasa S and Ando K 2012 Spin accumulation and spin lifetime in p-type germanium at room temperature *Appl. Phys. Express* **5** 53004
- [53] Weißhaupt D, Funk H S, Sürgers C, Fischer G, Oehme M, Schwarz D, Fischer I A, van Slageren J and Schulze J 2021 Formation of Mn5Ge3 on a recess-Etched Ge (111) quantum-well structure for semiconductor spintronics *Proc. 44th Int. Convention on Information, Communication and Electronic Technology (MIPRO)* (<https://doi.org/10.23919/MIPRO52101.2021.9596924>)
- [54] Sigle E, Weißhaupt D, Oehme M, Funk H S, Schwarz D, Berkmann F and Schulze J 2021 Strained Ge channels with high hole mobility grown on Si substrates by molecular

- beam epitaxy *Proc. 44th Int. Convention on Information, Communication and Electronic Technology (MIPRO)* (<https://doi.org/10.23919/MIPRO52101.2021.9597145>)
- [55] Oehme M, Kasper E, Weißhaupt D, Sigle E, Hersperger T, Wanitzek M and Schwarz D 2022 Two-dimensional hole gases in SiGeSn alloy *Semicond. Sci. Technol.* **37** 055009
- [56] White C R H *et al* 1990 The observation of the fractional quantum Hall effect in a single (AlGa)As/GaAs/(AlGa)As quantum well *Semicond. Sci. Technol.* **5** 792
- [57] Ponomarenko L A, de Lang D, de Visser A, Kulbachinskii V A, Galiev G B, Künzel H and Pruisken A 2004 The effect of carrier density gradients on magnetotransport data measured in Hall bar geometry *Solid State Commun.* **130** 705
- [58] Xu J *et al* 2019 Negative longitudinal magnetoresistance in gallium arsenide quantum wells *Nat. Commun.* **10** 287
- [59] Khan M A, Kuznia J N, van Hove J M, Pan N and Carter J 1992 Observation of a two-dimensional electron gas in low pressure metalorganic chemical vapor deposited GaN-Al_xGa_{1-x}N heterojunctions *Appl. Phys. Lett.* **60** 3027
- [60] Scholz F *et al* 1986 InP, GaInAs and quantum well structures grown by adduct MOVPE *J. Cryst. Growth* **77** 564
- [61] Bechler S, Kern M, Funk H S, Colston G, Fischer I A, Weißhaupt D, Myronov M, van Slageren J and Schulze J 2018 Formation of Mn₅Ge₃ by thermal annealing of evaporated Mn on doped Ge on Si(111) *Semicond. Sci. Technol.* **33** 95008
- [62] Funk H S, Kern M, Weißhaupt D, Sürgers C, Fischer I A, Oehme M, van Slageren J and Schulze J 2022 Composition and magnetic properties of thin films grown by interdiffusion of Mn and Sn-rich, Ge lattice matched Si_xGe_{1-x-y}Sn_y layers *J. Magn. Magn. Mater.* **546** 168731
- [63] Yamada N, Maeda K, Usami Y and Ohoyama T 1986 Magnetic properties of intermetallic compound Mn₁₁Ge₈ *J. Phys. Soc. Japan* **55** 3721
- [64] Arras E, Caliste D, Lançon F and Pochet P 2011 Phase diagram, structure, and magnetic properties of the Ge-Mn system: a first-principles study *Phys. Rev. B* **83** 174103
- [65] Tang J *et al* 2013 Electrical spin injection and detection in Mn₅Ge₃/Ge/Mn₅Ge₃ nanowire transistors *Nano Lett.* **13** 4036
- [66] Tang J *et al* 2012 Ferromagnetic germanide in Ge nanowire transistors for spintronics application *ACS Nano* **6** 5710
- [67] Sankar S, Beach R S and Berkowitz A E 1999 Exchange-biasing asymmetric spin valves using a pulsed current *Appl. Phys. Lett.* **75** 250
- [68] Yamada M, Naito T, Tsukahara M, Yamada S, Sawano K and Hamaya K 2018 Observation of local magnetoresistance signals in a SiGe-based lateral spin-valve device *Semicond. Sci. Technol.* **33** 114009
- [69] Morgunov R B, Kunitsyna E I, Talantsev A D, Koplak O V, Fache T, Lu Y and Mangin S 2019 Influence of the magnetic field sweeping rate on magnetic transitions in synthetic ferrimagnets with perpendicular anisotropy *Appl. Phys. Lett.* **114** 222402